Journal of Mechanical Science and Technology 29 (1) (2015) 191~198
www.springerlink.com/content/1738-494x
DOI 10.1007/s12206-014-1226-8

Modeling and control of lateral vibration of an axially translating flexible link †

Heonseop Shin and Sungsoo Rhim*

Department of Mechanical Engineering, Kyung Hee University, 1732 Deogyeong-daero, Yongin-si, Gyeonggi-do, 446-701, Korea

(Manuscript Received May 8, 2014; Revised September 30, 2014; Accepted September 30, 2014)

Abstract

Manipulators used for the transportation of large panel-shape payloads often adopt long and slender links (or forks) with translational joins to carry the payloads. As the size of the payload increases, the length of the links also increases to hold the payload securely. The increased length of the link inevitably amplifies the effect of the flexure in the link. Intuitively, the translational motion of the link in its longitudinal direction should have no effect on the lateral vibration of the link because of the orthogonality between the direction of the translational motion and the lateral vibration. If, however, the link was flexible and translated horizontally (perpendicular to the gravitational field) the asymmetric deflection of the link caused by gravity would break the orthogonality between the two directions, and the longitudinal motion of the link would excite lateral motion in the link. In this paper, the lateral oscillatory motion of the flexible link in a large-scale solar cell panel handling robot is investigated where the links carry the panel in its longitudinal direction. The Newtonian approach in conjunction with the assumed modes method is used for derivation of the equation of motion for the flexible forks where non-zero control force is applied at the base of the link. The analysis illustrates the effect of longitudinal motion on the lateral vibration and dynamic stiffening effect (variation of the natural frequency) of the link due to the translational velocity. Lateral vibration behavior is simulated using the derived equations of the motion. A robust vibration control scheme, the input shaping filter technique, is implemented on the model and the effectiveness of the scheme is verified numerically.

Keywords: Flexible link; Axial motion; Lateral vibration; Dynamic stiffening; Vibration control

---

1. Introduction

Flexible links with translational joints have been adopted in many motion systems, for example, the large-scale solar cell panel handling manipulators shown in Figs. 1(a) and (b), where the long and slender forks transport the heavy solar cell panel in the longitudinal direction of the forks. In these systems, vibration in the lateral direction of the links (or forks) perpendicular to the direction of the translational motion of the links (or forks) deteriorates the performance of the whole machine.

Intuitively, lateral vibration during translation of a flexible link should not occur due to the orthogonal relationship between the translating direction (input) and the lateral vibration direction (output). Due to the deflection caused by the flexure of the link and gravitational effect, however, the slope of the link becomes a non-horizontal line such that input direction becomes non-orthogonal to the output direction. Furthermore, as it is to be explained in the following sections longitudinal motion could change the compliance of the lateral motion (which is often called dynamic stiffening and softening effects).

These complex dynamic problems are becoming more severe, since the trend in robot design is toward light and speedy systems.

To reduce lateral vibration due to longitudinal motion and improve the performance of the robot mentioned above, an investigation is required to analyze the dynamics and the controllability of this system. To explore the basic nature of the rotating/translating flexible link behavior and control of lateral vibration, various studies have been carried out. Behavior of a flexible cantilever beam on a moving base was investigated using Kane's equation [1-4]. Furthermore, the concept of the dynamic stiffening effect was first introduced in Ref. [1]. Dynamic stability analysis was previously performed by employing the perturbation method [2]. Through expression of strain energy in quadratic form, the stiffness variation was accurately captured [3]. In Ref. [4], dynamic stiffening and softening effects were intensively studied for the rotating bodies, and their relationship with frequency was introduced.

Also, the significance of stiffening effects in rotating flexible multibody dynamic systems were previously studied and verified with experimental results [5]. An equation of motion was derived for a similar system by using the energy method [6]. Pratiher [7] obtained an approximate solution by using a

---

*Corresponding author. Tel.: +82 31 201 3248, Fax.: +82 31 202 8106
E-mail address: ssrhim@khu.ac.kr
† Recommended by Editor Yeon June Kang

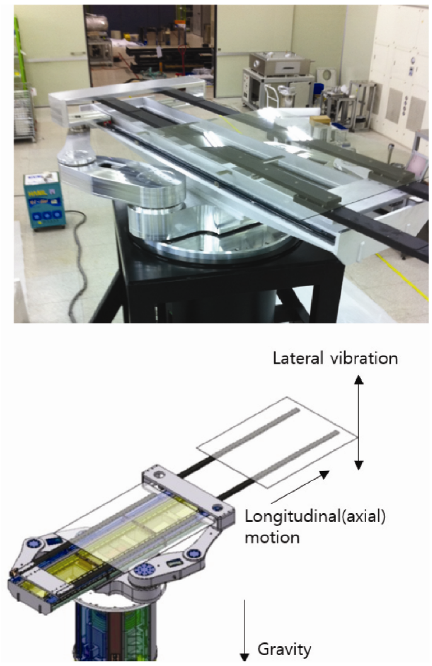

Fig. 1. Solar-cell panel transportation robot with flexible links (or forks).

perturbation method and performed vibration control. The vibration of rotating beam systems has long been studied [8-12]. All systems mentioned above are based on a cantilever beam model acting on an axial force. In Refs. [14-16], the effect of an axial load on system frequency was investigated.

Most actual implementations in real systems employ an open-loop control approach for the effectiveness and the stability concern. The time-delayed command (input) shaping technique is one of the open-loop control schemes that are widely used to reduce vibration in the motion system [17-24]. There have been studies regarding the input shaping technique and its application. A ZV (zero vibration) shaping filter is a basic form of the delayed input shaping technique developed for the flexible system [17] and its effectiveness has bee verified in various applications [18]. Multi-hump EI (extra-insensitive) input shaping filters were introduced for the improved robustness and their effectiveness was verified [19, 20]. In order to deal with unknown or varying system parameters, adaptive and learning command shaping filters were developed as well [21, 22].

The aim of this work is to reduce the lateral vibration of an axially translating flexible link considering the frequency variation due to the dynamic stiffening effects. An equation of motion the translating link with lateral vibration is derived using Newtonian approach to analyze the influence of translating motion to lateral vibration and a numerical simulation is using the derived equations. Then the input shaping control method is applied to the model. Numerical analysis results are shown and discussed to show the effectiveness of the control approach in the presence of the pseudo-orthogonal relationship between the input and output and also the frequency variation due to the dynamic stiffening effect.

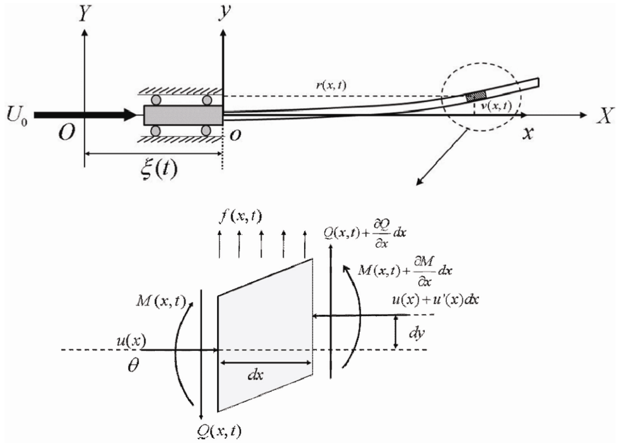

Fig. 2. Schematic drawing of the system and the free-body diagram of infinitesimal element.

2. Mathematical modeling and equation of motion

2.1 Modeling

A schematic drawing of a translating flexible link to be discussed in this paper is shown in Fig. 2, where the base of the link is horizontally sliding, and the tip of the link is free to move. The frame *O-X-Y* is fixed on the ground and the moving frame *o-x-y* is attached at the base and moves along with the base. In Fig. 2, U_0 is the actuation input force applied on the base, and $\zeta(t)$ represents the displacement of the base along with axis X.

Fig. 2 also shows the forces and moments acting on an infinitesimal element of the link. $Q(x,t)$ and $M(x,t)$ are shear force and moment acting on the element, respectively. $f(x)$ represents the gravitational force acting on the element; $r(x,t)$ and $v(x,t)$ represent axial displacement and lateral displacement, respectively. From the force-momentum equilibrium, Eqs. (1)-(3) can be obtained:

$$\sum F_X : u(x) - \left(u(x) + u'(x)dx\right) = \rho A dx \frac{\partial^2 r}{\partial t^2} \quad \Leftrightarrow \quad -u'(x) = \rho A \frac{\partial^2 r}{\partial t^2} \tag{1}$$

$$\sum F_Y : (-Q) + \left(Q + \frac{\partial Q}{\partial x}dx\right) + f dx = \rho A dx \frac{\partial^2 v}{\partial t^2} \quad \Leftrightarrow \quad \frac{\partial Q}{\partial x} + f = \rho A \frac{\partial^2 v}{\partial t^2} \tag{2}$$

$$\sum M_Z : \left(M + \frac{\partial M}{\partial x}dx\right) - M + \left(Q + \frac{\partial Q}{\partial x}dx\right)dx + \left(u(x) + u'(x)dx\right)dy = 0 \quad \Leftrightarrow \quad Q = -\frac{\partial M}{\partial x} - u(x)\frac{\partial y}{\partial x} \tag{3}$$

where ρ is the mass density, A is the cross-section area of the link, $X = \xi(t) + x$, and $u'(x) = du(x)/dx$. Also, the axial force $u(x)$ acting on the element at a given position is assumed to follow Eq. (4), and then it would satisfy the force boundary condition at both ends of the link.

$$u(x) = \frac{(L-x)}{L}U_0 \qquad 0 \le x \le L \tag{4}$$

where L is the length of the link. By substituting Eq. (3) into Eq. (2) and using the moment and curvature relation, we can rewrite Eqs. (1) and (2) as

$$\rho A \frac{\partial^2 r(x,t)}{\partial t^2} = \frac{U_0}{L} \tag{5}$$

$$\begin{aligned} &\rho A \frac{\partial^2 v(x,t)}{\partial t^2} + EI\frac{\partial^4 v(x,t)}{\partial x^4} + u(x)\frac{\partial^2 v(x,t)}{\partial x^2} \\ &\quad + u'(x)\frac{\partial v(x,t)}{\partial x} - f(x,t) = 0 \end{aligned} \tag{6}$$

where E is Young's modulus and I is the moment of inertia of the link. Utilizing this method of separation of variables, the solutions of Eqs. (5) and (6) may be represented as:

$$r(x,t) = \eta(t)\psi(x) \tag{7}$$

$$v(x,t) = \alpha(t)\phi(x) \tag{8}$$

where $\eta(t)$ and $\alpha(t)$ are time-dependent functions, and $\psi(x)$ and $\phi(x)$ are space-dependent shape functions.

2.2 Translational motion

With the assumption of ignorable longitudinal vibration (rigid in the direction of the translation), $\psi(x)$ in Eq. (7) becomes

$$\psi(x) = 1 . \tag{9}$$

Substituting Eq. (9) into Eq. (7) and inserting the result into Eq. (5) gives

$$\frac{d^2\eta(t)}{dt^2} = \frac{U_0}{\rho AL} . \tag{10}$$

Integrating Eq. (10) with respect to time and introducing it into Eq. (7) we obtain

$$r(x,t) = \eta(t) = \frac{U_0}{\rho AL}t^2 . \tag{11}$$

The displacement of the base relative to the fixed frame O-X-Y, $\xi(t)$, is calculated as follows

$$\xi(t) = \frac{U_0}{\rho AL}t^2 . \tag{12}$$

2.3 Shape function of lateral vibration

The shape function $\phi(x)$ can be obtained by solving Eq. (13), which results from substituting Eq. (8) into Eq. (6) with $f(x,t) = 0$

$$\begin{aligned} m\phi(x)\ddot{\alpha}(t) + \Big\{&EI\phi^{(4)}(x) + u(x)\phi^{(2)}(x) \\ &+ u'(x)\phi^{(1)}(x)\Big\}\alpha(t) = 0 \end{aligned} \tag{13}$$

where $m = \rho A$ denotes the mass of the link per unit length, $\ddot{\alpha}(t) = d^2\alpha(t)/dt^2$, $\phi^{(n)} = d^n\phi(x)/dx^n$ and so forth. Dividing both sides of Eq. (13) by $m\alpha(t)\phi(x)$ we obtain

$$\frac{\ddot{\alpha}(t)}{\alpha(t)} = -\frac{1}{m\phi(x)}\left\{EI\phi^{(4)}(x) + u(x)\phi^{(2)}(x) + u'(x)\phi'(x)\right\} . \tag{14}$$

Since x and t are independent variables, each side of Eq. (14) must be constant. Then, the left side of Eq. (14) can be rewritten

$$\ddot{\alpha}(t) - \lambda\alpha(t) = 0 \tag{15}$$

where λ is a constant. The general solution to Eq. (16) can be expressed as Eq. (16)

$$\alpha(t) = C\cos(\omega t - \theta) \tag{16}$$

where ω is the natural frequency of oscillation ($\omega^2 = -\lambda$), C is an amplitude and θ is a phase angle. Substituting Eq. (16) into Eq. (13) gives

$$\begin{aligned} &\phi^{(4)} + \frac{u(x)}{EI}\phi^{(2)} + \frac{u'(x)}{EI}\phi^{(1)} - \frac{m\omega^2}{EI}\phi = 0 \\ &\Leftrightarrow \phi^{(4)} + \left(\frac{L-x}{LEI}\right)U_0\phi^{(2)} - \frac{U_0}{LEI}\phi^{(1)} - \frac{m\omega^2}{EI}\phi = 0 \end{aligned} . \tag{17}$$

It is interesting to note that the second term on the left-side in Eq. (17) represents the effect of the axial force on the shape function and makes the equation non-linear. To simplify the 4th order non-linear partial differential equation which is not easily solvable, it can be assumed that the effect of axial force on the shape function is negligible [14, 15]. Although a difference does exist between the current system and the axially loaded beam model studied in Refs. [14, 15], a considerably similar equation for the shape function is obtained indicates that the effect of the axial load on the shape function is negligible for a small axial force. Fig. 3 shows the small variation of the shape functions for the axially loaded beam [14, 15], indicating that the axial force does not seriously affect the shape function. Therefore, the second and the third terms of Eq. (17) are assumed to be negligible and the shape function is derived from Eq. (18).

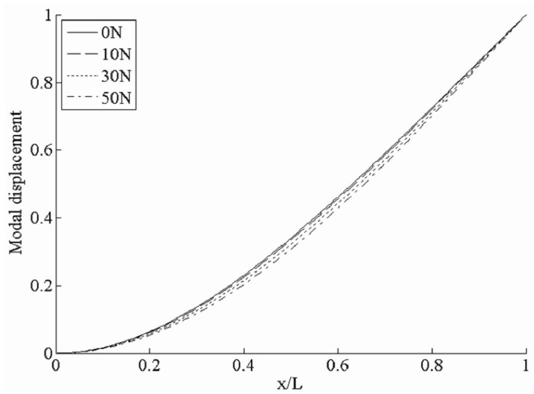

(a) 1st mode

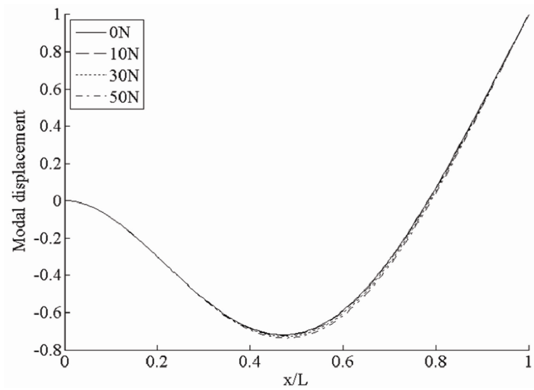

(b) 2nd mode

Fig. 3. Effect of various axial forces on mode shapes in axially loaded beam ($m = 4$ kg, $L = 1.8$ m, $E = 69$ Gpa, $I = 6.66\ 10^{-9}$ m^4, $A = 0.0008$ m^2).

$$\phi^{(4)}(x) + \frac{U_0}{EI}\phi^{(2)}(x) - \frac{m\omega^2}{EI}\phi(x) = 0\,. \tag{18}$$

Applying the 'clamped-free' boundary conditions listed in Eq. (19) and Eq. (20) to Eq. (18), we can obtain the general solution to Eq. (18) as

$$\phi(x) = 0\,,\ \ \phi^{(1)}(x) = 0 \ \text{ at } \ x = 0 \tag{19}$$

$$Q(x) = \phi^{(3)}(x) = 0\,,\ \ M(x) = \phi^{(2)}(x) = 0 \ \text{ at } \ x = L \tag{20}$$

$$\phi_r(x) = A_r\big[\sin\beta_r(x) - \sinh\beta_r(x) - h_r\left\{\cos\beta_r(x) - \cosh_r(x)\right\}\big] \qquad r = 1,2,3\ldots\infty \tag{21}$$

where β_r is the solution to the characteristic equation $\cos\beta L\cosh\beta L + 1 = 0$, and the constant coefficient A_r would be determined by satisfying the orthonormality of eigenfunctions and $h_r = (\sin\beta_r L + \sinh\beta_r L)/(\cos\beta_r L + \cosh\beta_r L)$.

2.4 Approximate solution

The approximate solution to Eq. (13) is assumed based on the Rayleigh-Ritz method as follows

$$y(x,t) = \sum_{j=1}^{N}\alpha_j(t)\phi_j(x)\,. \tag{22}$$

Substituting Eq. (22) into Eq. (6) we get

$$\sum_{j=1}^{N}\left\{\rho A\ddot{\alpha}_j\phi_j + EI\alpha_j\phi_j^{(4)} + u(x)\alpha_j\phi^{(2)} + u'(x)\alpha_j\phi_j^{(1)}\right\} = f\,. \tag{23}$$

Multiplying the both sides of Eq. (23) with $\phi_m(x)$ and integrating over the length of the link and making use of the orthonormality property of $\phi_m(x)$, we can obtain a linear time-varying ordinary differential equation for $\alpha_m(t)$:

$$\ddot{\alpha}_m + k_{mm}\alpha_m = \int_0^L f\phi_m dx + \sum_{j=1, j\neq m}^{N} k_{jm}\alpha_j \tag{24}$$

where

$$k_{mm} = \int_{x_0}^{x_L}\left\{EI\phi_m{}^{(4)} + u(x)\phi_m{}^{(2)} + u'(x)\phi_m{}^{(1)}\right\}\phi_m dx,$$

$$k_{jm} = \int_{x_0}^{x_L}\left\{EI\phi_j{}^{(4)} + u(x)\phi_j{}^{(2)} + u'(x)\phi_j{}^{(1)}\right\}\phi_m dx$$

and $m = 1,2,\cdots,N$. For better understanding of axial motion, k_{mm} and k_{jm} can be rewritten as:

$$k_{mm} = \int_0^L\left\{EI\phi_m{}^{(4)} + \left(\frac{L-x}{L}\right)\rho ALa_{U_0}\phi_m{}^{(2)} - \rho Aa_{U_0}\phi_m{}^{(1)}\right\}\phi_m dx, \tag{25}$$

$$k_{jm} = \int_0^L\left\{EI\phi_j{}^{(4)} + \left(\frac{L-x}{L}\right)\rho ALa_{U_0}\phi_j{}^{(2)} - \rho Aa_{U_0}\phi_j{}^{(1)}\right\}\phi_m dx \tag{26}$$

where a_{u_0} is the acceleration of the link caused by U_0 in the axial direction. It is noteworthy that the time function, α_m is affected by the acceleration of the link, a_{u_0}, whose effect on vibration is shown in the following section. For a better representation of the actual system behavior, a simple linear damping model is added, and we obtain the equation of the time functions as follows:

$$\ddot{\alpha}_m + v_m\dot{\alpha}_m + k_{mm}\alpha_m = \int_0^L f\phi_m dx + \sum_{j=1, j\neq m}^{N} k_{jm}\alpha_j \tag{27}$$

where v_m is the damping coefficient to the m^{th} mode.

3. Dynamic analysis

It is evident that the coefficient of α_m in Eqs. (24) and

(27) represents the stiffness of the flexible link, and it contains the axial force. Consequently, the natural frequency of the link varies along with the axial force. The variation of the stiffness due to the motion of the link is sometimes called the dynamic stiffening/softening effect, and it has been studied in a rotating system [1, 4]. Previous studies have modeled this system with Kane's equation, but do not explain in detail what and how component properties of the system affect the dynamic stiffening effect. In this paper, the equation of motion is derived with a Newtonian approach, which is a more direct method of investigating the relationship between the system properties and the dynamic stiffening effect. The natural frequency of the n^{th} elastic mode of the link when the link translates at a constant speed is called the base natural frequency, $\omega_{n.b}$, and it is expressed as follows:

$$\omega_{n.b} = \left(\int_{x_0}^{x_L} EI\phi^{(4)}\phi dx \right)^{\frac{1}{2}}. \tag{28}$$

Then, the variable natural frequency of the n^{th} elastic mode is expressed using $\omega_{n.b}$ as follows:

$$\omega_n = \left[{\omega_{n.b}}^2 + \int_0^L \rho A a_{U_0} \left\{ (L-x) L {\phi_m}^{(2)} - {\phi_m}^{(1)} \right\} \phi_m dx \right]^{\frac{1}{2}} \tag{29}$$

where $a_{U_0.cr}$ is critical acceleration that makes the frequency zero in analytical derivation. Eq. (29) explicitly shows that the translational acceleration affects ω_n and is not equal to $\omega_{n.b}$. The dynamic stiffening effect is basically invoked by the additional moment resulting from the offset of the link elements from the axial centerline, which is represented as dy in Fig. 2. The offset from the centerline, which acts as the moment arm, is primarily generated by the vertical deflection of the link. It would be interesting to investigate the effect of the deflection of the link on the dynamic stiffening phenomena. Let us here introduce a new parameter, the deflection ratio defined as:

$$\kappa = \frac{initial\, static\, deflection}{L} = \frac{\rho A L^3}{8EI}. \tag{30}$$

The deflection ratio, κ, represents the effective compliance of the link. Combining Eq. (29) with Eq. (30) gives

$$\omega_n = \left[{\omega_{n.b}}^2 + \int_0^L \frac{8\kappa EI}{L^3} a_{U_0} \left\{ (L-x) {\phi_m}^{(2)} - {\phi_m}^{(1)} \right\} \phi_m dx \right]^{\frac{1}{2}}. \tag{31}$$

Examples of the frequency variation tendency of a translating link are calculated using Eq. (31) as a function of κ, and the results for $\kappa = 0.02$, 0.04, 0.06, 0.08 and 0.10 are shown in Fig. 4. In the example, the system parameters are assumed to be $E = 69$ Gpa, $L = 1.8$ m, $\rho = 2770$ kg/m^3, and width of the cross-section of the link $= 0.08m$. The height and the width of the cross-section of the link are determined per κ value using Eq. (30) listed above.

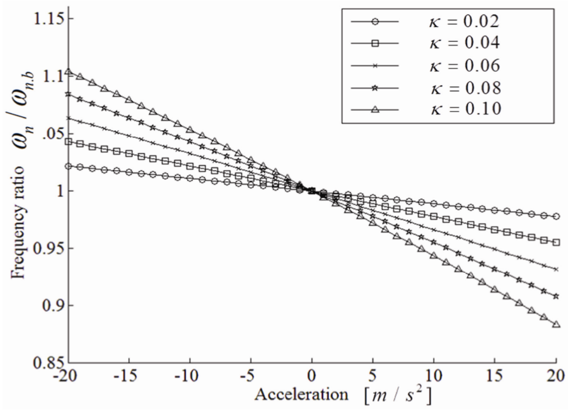

Fig. 4. Effect of axial mode and elasticity on frequency variation.

As shown in Fig. 4, κ affects the natural frequency of the system, and as the κ value of the system increases, more variation in the natural frequency will result for the same given translational acceleration. The plot shown in Fig. 4 normalizes the frequency variation of a given link based on the κ value and it helps us to anticipate the frequency range of the system without going through a complicated dynamic analysis. The information in the plot is useful for the design of an effective vibration control system.

4. Vibration control using input shaping

An input shaping filter is an open-loop control algorithm, which modifies the input trajectory to suppress the vibration. The input shaping filter reshapes the input trajectory without changing the DC gain of the trajectory and removes the excitation energy at the target frequency from the original trajectory. The control technique is widely used in vibration suppression control for its effectiveness and the robustness of the system parameters [19-24].

Since the introduction of the fundamental concept of the input shaping technique, several types of input shaping filters have been designed and used for various motions systems. The basic form of the shaping filter is often called a 'zero-vibration (ZV)' filter, which has a narrow working frequency range for the fixed vibration frequency system [17].

If a frequency of the system is not given or is variable, the performance of the input shaper becomes less effective. In order to increase the robustness of the filter, various input shaping filters have been designed, including the multi-hump positive impulse extra-intensity (EI) input shaping filter [20]. The sensitivity and robustness of the input shaping filter are represented by the width and magnitude of the stop-band in the frequency domain. The lower the magnitude of the frequency response of the filter at the stopband becomes, the

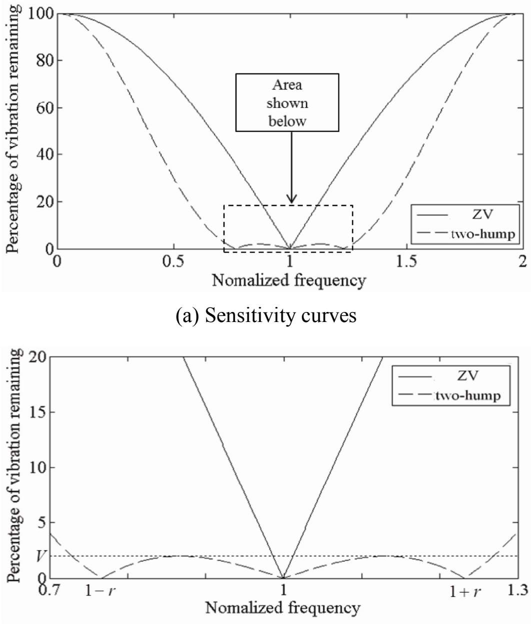

(a) Sensitivity curves

(b) Magnified plot

Fig. 5. Sensitivity curves of ZV input shaping filter and two-hump EI input filter.

lower the amplitude of the residual vibration of that frequency. For wider stopband frequency responses, uncertainty (or the variation) in the target frequency increases, resulting in the increased response of the filter. Fig. 7 compares the sensitivity curves of the typical ZV input shaping filter and the two-hump EI input shaping filters. In the figure, it is apparent that the two-hump EI shaper has a wider stopband, but has a higher magnitude at the stopband. This means more excitation energy will remain in the filtered trajectory and more residual vibration will be excited in the system in that frequency range.

Based on the analysis results shown previously, the EI shaper would be more appropriate for the translating flexible link system, which has a varying vibration frequency. In this paper, an effective two-hump EI filter is designed to suppress the lateral vibration of the axially translating flexible link. An effective two-hump EI input shaping filter can be designed from the system parameters as follows [20].

$$H(e^{j\omega_{n.b}}) = c_0 + c_1 \cdot e^{-\Delta T j\omega_{n.b}} + c_2 \cdot e^{-2\Delta T j\omega_{n.b}} + c_3 \cdot e^{-3\Delta T j\omega_{n.b}} \tag{32}$$

where

$$c_0 = \frac{3X^2 + 2X + 3V^2}{16X}, c_1 = \frac{1}{2} - c_0, \ c_2 = c_1, \ c_3 = c_0,$$

$$\sum_{i=0}^{3} c_i = 1 \tag{33}$$

$$X = \sqrt[3]{V^2(\sqrt{1-V^2}+1)} \tag{34}$$

$$\Delta T = \frac{\pi}{\omega_{n.b}}. \tag{35}$$

As shown in Eqs. (32)-(35), the design of an effective EI filter requires the determination of the target frequency, the range of effective frequency range, and the pass-through magnitude V (or the maximum magnitude of the stopband in the sensitivity curve within that range). In this study, the target frequency is set to $\omega_{n.b}$. The sensitivity, V, and the range of effective target frequency, r, are coupled, and only one of them can be chosen freely. The choice of a large value of V results in a wider range. In this study, the pair of (V, r) is chosen to ensure that the range of r includes the variation range of the natural frequency of the flexible link system. The effectiveness of the two-hump EI input shaping filter is compared with the ZV filter in the next section.

5. Simulation results

The numerical simulation of the dynamic behavior of a flexible link translating on a horizontal plane was performed using the equations of motion derived in the previous section. The system parameters were assumed to be E = 69 *Gpa*, L = 1.8 *m*, and ρ = 2770 kg/m^3. The width of the cross-section of the link is set, and the height of the cross-section of the link is chosen to produce $\kappa = 0.10$. The accuracy of the simulation model would increase as the number of elastic modes included in the simulation model increases but the improvement in accuracy significantly decreases after the second elastic mode. Therefore, only the first two elastic modes are considered for the simulation without losing the validity.

Fig. 6 shows the lateral vibration response to the step-force axial translation input given at the base of the link. Plot (a) in Fig. 6 shows the acceleration step input of the longitudinal translational motion of the base. Fig. 6(b) depicts the response of the system model without damping, while Fig. 6(c) represents the response of the system model with damping. In both plots, it is apparent that the period and the amplitude of the vibration increase as the input force (or the axial acceleration) increases. In both plots, larger acceleration results in larger fluctuation. An interesting result found in Fig. 6(b) is that for greater acceleration of the translation, a larger steady state deformation is observed after the transient vibration dies out.

The vibration suppression controllers using input shaping filters are designed and implemented in the simulation for various system parameters, and very consistent results are obtained. In this paper, only a single set of simulation results from a flexible link with the deflection ratio $\kappa = 0.10$ is included. Fig. 7 shows the lateral vibration responses of the link for the motion cases with no input shaping filter, ZV filters, and two-hump EI filters.

Plot (a) in Fig. 7 shows the acceleration ramp input of the longitudinal translational motion of the base. As explained in Eqs. (24)-(26), the variation in the acceleration (ramp signal) during the motion causes a dynamic stiffening effect in the

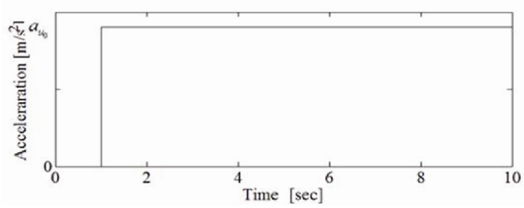

(a) Acceleration input for longitudinal motion

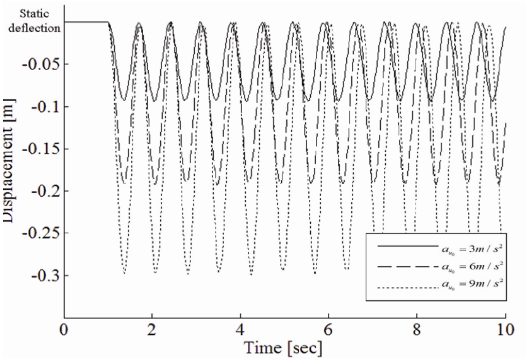

(b) Lateral vibration from model without damping

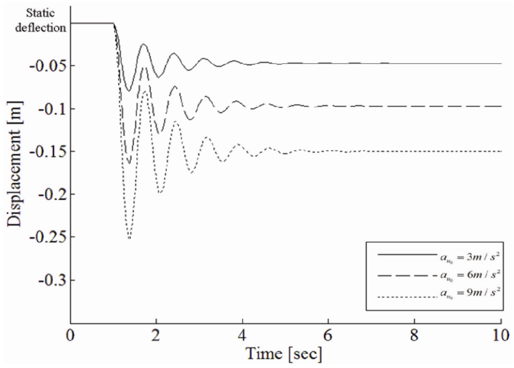

(c) Lateral vibration from model with damping

Fig. 6. Effect of acceleration from model with damping.

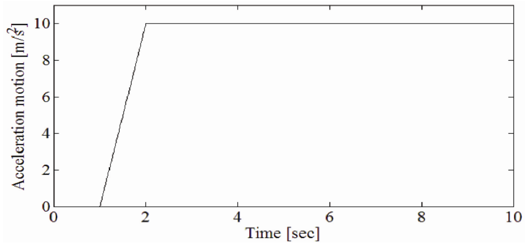

(a) Acceleration input for longitudinal motion

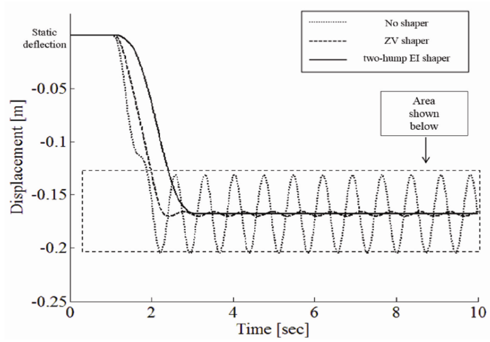

(b) Lateral vibrations with no-filter, ZV filters, EI shapers

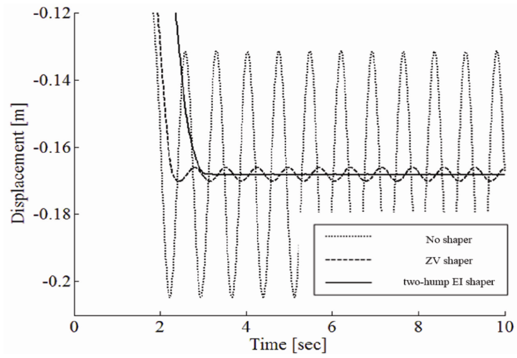

(c) Lateral vibrations with no-filter, ZV filters, EI shapers (magnified)

Fig. 7. Simulation results of vibration control with various shaping filters.

link, and the natural frequency of the lateral vibration varies during the motion between 0.9436 and 1 times $\omega_{n.b}$. The two ZV filters are designed to target the natural frequency of the first two elastic modes, $\omega_{1.b}$ and $\omega_{2.b}$. Two two-hump EI filters were designed with target frequencies at $\omega_{1.b}$ and $\omega_{2.b}$, and the sensitivity magnitude was set to V = 0.001 so the effective frequency range r would cover the frequency variation range explained above.

6. Conclusion

The longitudinal (axial) motion of the link is considered to be decoupled completely from the lateral vibration in normal cases. However, with the presence of non-ignorable flexure (or the consequent deformation) of the link, the longitudinal motion is coupled with the lateral vibration. A light-weight slender link used to transport a large, heavy panel in the horizontal plane would result in the deflection of the link in the vertical direction, and the axial translation of the link excites the lateral vibration of the link.

The coupling dynamics between the longitudinal motion and the lateral vibration of the flexible link are analyzed and the equations of motion are derived using the Newtonian approach. In particular, the frequency variation of the lateral vibration due to the acceleration change of the axial motion is analyzed using the dynamic stiffening effect mathematically modeled in the equations of the motion. The frequency variation tendency is mathematically formulated using a newly introduced system parameter, the deflection ratio, to estimate the frequency variation range. Knowing the frequency variation range would be very helpful in designing a vibration control system for lateral vibration.

A vibration controller using the input shaping technique is designed to reduce the lateral vibration induced by the longitudinal motion. The effectiveness of the vibration controller is verified by simulation. Two-hump EI shapers and ZV shapers are implemented to reshape the reference trajectory of the longitudinal motion of the flexible link, and the simulation results indicate that the reshaped longitudinal reference input reduces the amplitude of the lateral vibration down to less than 10% of the original amplitude. Due to the frequency variation of the system during the longitudinal translation, the EI shaper results in better suppression of the vibration than the ZV shaper.

Acknowledgement

This work was supported by the research project (No. 10035218) funded by the Ministry of Trade, Industry and Energy, Korea.

References

[1] T. Kane, R. Ryan and A. Banerjee, Dynamics of a cantilever beam attached to a moving base, *Journal of Guidance Control Dynamics*, 10 (2) (1987) 139-151.

[2] S. H. Hyun and H. H. Yoo, Dynamic modelling and stability analysis of axially oscillating cantilever beams, *Journal of Sound and Vibration*, 228 (3) (1999) 543-558.

[3] H. H. Yoo, R. R. Ryan and R. A. Scott, Dynamics of flexible beams undergoing overall motions, *Journal of Sound and Vibration*, 2004, 181 (2) (1995) 261-278.

[4] S. F. Xiao and B. Chen, Dynamic characteristic and stability analysis of a beam mounted on a moving rigid body, *Journal of Applied Mechanic*, 74 (5-6) (2005) 415-426.

[5] J. Rhu, S.-S. Kim and S.-S. Kim, Flexible multibody dynamic system simulation, *Computers and Structures*, 62 (6) (1997) 1035-1048.

[6] M. Vakil, E. Sharbati, A. Vakil, F. Heidari and R. Fotouhi, Vibration analysis of a Timoshenko beam on a moving base, *Journal of Vibration and Control*, 0 (0) 1-18.

[7] B. Pratiher, Vibration control of a transversely excited cantilever beam with tip mass, *Journal of Applied Mechanic*, 82 (1) (2011) 31-42.

[8] A. Yigit, R. Scott and G. Ulsoy, A, Flexural motion of a radially rotating beam attached to a rigid body, *Journal of Sound and Vibration*, 121 (2) (1988) 201-210.

[9] A. M. Bloch, Stability analysis of a rotating flexible system, *Journal of Acta Applicandae Mathemeticae*, 15 (3) (1989) 211-234.

[10] S. B. Choi, C. C. Cheong and H. C. Shin, Sliding mode control of vibration in a single-link flexible arm with parameter variation, *Journal of Sound and Vibration*, 179 (5) (1995) 737-748.

[11] J. B. Yang, L. J. Jiang and D. C. Chen, Dynamic modeling and control of a rotating Euler-Bernoulli beam, *Journal of Sound and Vibration*, 274 (3-5) (2004) 863-875.

[12] S. Bai, P. Ben-Tzvi, Q. Zhou and X. Huang, Dynamic modeling of a rotating beam having a tip mass, *ROSE 2008 IEEE* (2008) 17-18.

[13] A. K. Banerjee and J. M. Dickens, Dynamics of an arbitrary flexible body in large rotation and translation, *Journal of Guidance*, 13 (2) (1990) 221-227.

[14] F. J. Shaker, Effect of axial load on mode shapes and frequencies of beams, *Lewis Research Center Report NASA* (1975).

[15] A. Bokaian, Natural frequencies of beams under compressive axial loads, *Journal of Sound and Vibration*, 126 (1) (1988) 49-65.

[16] H. Ding and L.-Q. Chen, Natural frequencies of nonlinear vibration of axially moving beams, *Journal of Nonlinear Dynamics*, 63 (1-2) (2011) 125-134.

[17] N. C. Singer and W. P. Seering, Preshaping command inputs to reduce system vibration, *J. of Dynamic Systems, Measurement, and Control*, 112 (1) (1990) 76-82.

[18] D. P. Magee and W. J. Book, Experimental verification of modified command shaping using a flexible manipulator, *International Conference on Motion and Vibration Control*, Japan (1992) 553-558.

[19] W. Singhose, L. J. Porter and N. C. Singer, Vibration reduction using multi-hump extra-insensitive input shapers, *Proceedings of the American Control Conference*, Seattle (1995).

[20] W. Singhose, L. Porter, T. D. Tuttle and N. C. Singer, Vibration reduction using multi-hump input shapers, *Journal of Dynamic Systems, Measurement, and Control*, 119 (2) (1997) 320-326.

[21] S. Rhim, N. Sadegh and W. J. Book, Combining a multirate repetitive learning controller with command shaping for improved flexible manipulator control, *Journal of Dynamic Systems, Measurement, and Control*, 123 (3) (1999) 385-390.

[22] S. Rhim and W. J. Book, Adaptive time-delay command shaping filter for flexible manipulators, *IEEE/ASME Transactions on Mechatronics*, 9 (4) (2004) 619-626.

[23] W. Singhose, L. Porter, M. Kenison and E. Kriikku, Effects of hoisting on the input shaping control of gantry cranes, *Journal of Control Engineering Practice*, 8 (10) (2000) 1159-1165.

[24] W. Singhose, Command shaping for flexible systems: A review of the first 50 years, *Journal of Precision Engineering and Manufacturing*, 10 (4) (2009) 153-1.

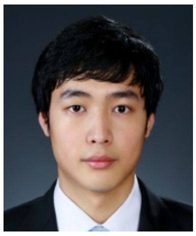

Heonseop Shin received his B.S. and M.S. degrees (with highest honor for M.S.) in Mechanical Engineering from Kyung Hee Univ., Korea, in 2012 and 2014, respectively. He is currently a doctoral student at the Dept. of Mechanical Engineering in Kyung Hee Univ., Korea. His research interests are theoretical studies in flexible link vibration analysis, vibration control and contact mechanics.

Sungsoo Rhim received his B.S. and M.S. degrees in Mechanical Engineering from Seoul National Univ., Korea, in 1990 and 1992, respectively. He received his Ph.D. degree in mechanical engineering from Georgia Institute of Technology in 2000. He is currently an Associate Professor at the Dept. of Mechanical Engineering in Kyung Hee Univ., Korea. His research interests include system dynamics and control of robotic systems.